International Journal of Smart Grid (IJSmartGrid)
https://www.ijsmartgrid.org/ Online ISSN: 2602-439X
A. Tatish and K. Vaisakh., Vol. 10, No. 1, March, 2026 Research Article

Simplified Finite-Control-Set Model Predictive Control for Grid-Connected Inverters with LCL Filters: Reduced Prediction Horizon and Weighting Factors-Free Design

Adel Tatish *‡, Kanchapogu Vaisakh *

* Department of Electrical Engineering, Andhra university, Visakhapatnam 530017, AP, India

(adeltatish.rs@andhrauniversity.edu.in, prof.kvaisakh@andhrauniversity.edu.in)

‡ Corresponding Author; Andhra university, Visakhapatnam 530017, AP, India Tel: +917567627748,

adeltatish.rs@andhrauniversity.edu.in

Received: 28.08.2025 Accepted:23.11.2025

Abstract- Finite-Control-Set Model Predictive Control (FCS-MPC) has shown great promise for controlling microgrid converters. However, conventional FCS-MPC approaches applied to high-order dynamic systems, such as grid-connected converters with LCL filters, require a long prediction horizon to achieve accurate grid current tracking, resulting in increased computational burden. This paper proposes a simplified FCS-MPC strategy for grid-connected inverters with LCL filters, addressing the computational complexity and tuning challenges of conventional methods. By tracking the filter capacitor voltage instead of directly regulating grid-side or converter-side currents, the proposed approach reduces the required prediction horizon from six steps (Np=6) to three steps (Np=3), significantly lowering computational burden. This reduction, coupled with a single-objective cost function, slashes the computational time by over 300 times, from 7.8 ms to 25.3 µs on embedded hardware (400 MHz CPU), making real-time implementation feasible. A single-objective cost function eliminates the need for weighting factors, simplifying controller design and tuning. The method ensures sinusoidal current injection even under unbalanced grid conditions by exclusively utilizing the positive sequence of the PCC voltage, extracted via a discrete-time quadrature signal generator. The effectiveness of the proposed strategy is validated through both MATLAB/Simulink simulations and experimental testing. The results demonstrate that the proposed controller achieves performance comparable to conventional FCS-MPC approaches with longer prediction horizons, maintaining a low grid-current THD of 1.7%, while offering the distinct advantages of reduced computational complexity, improved robustness against grid harmonics and voltage sags, and simpler implementation without the need for tuning weighting factors.

Keywords Grid following inverter, LCL filter, finite-control-set model predictive control (FCS-MPC), prediction horizon.

1. Introduction

Conventional power systems are structured to allow power flow from central plants to transmission and distribution systems. However, the increasing quest to benefit from renewable energy sources (RES) has prompted many developed countries to change the power system's structure to suit the new grid's requirements with high penetration of RES [1]. Furthermore, microgrids emerged and spread widely as one of the solutions for integrating distributed generation (DG) systems based on RES into conventional power systems, apart from their notable role in enhancing reliability,

Cite this article as: A. Tatish and K. Vaisakh, "Simplified Finite-Control-Set Model Predictive Control for Grid-Connected Inverters with LCL Filters: Reduced Prediction Horizon and Weighting Factors-Free Design" *International Journal of Smart Grid (ijSmartGrid)*, Vol. 10, No. 1, pp. 1–13, March, 2026.

flexibility, economical operation, and optimal use of distributed energy resources [2].

Grid-connected inverters (GCI) play a crucial role in microgrids as they serve as power interfaces that facilitate the integration of DG units into the utility grid and contribute with several advantageous characteristics, including controlling active and reactive power flow and injecting high-quality current into the grid [3], [4]. In this work, we focus on voltage-source inverters (VSIs), which are widely adopted in industrial applications due to their simple structure, compatibility with LCL filters, and ease of modulation [5], [6]. The simple two-level inverter topology is most favored among the various inverter topologies due to its simple operating principle, basic structure, and extensive industrial utilization [7] [8]. The researchers have developed several control strategies for GCIs. Among these strategies, simple control strategies like traditional PID-based controllers and PR-based controllers are widely employed for GCI applications [2], [4], and [9]. However, these approaches possess certain limitations [8], [10]. The control structure, consisting of multiple complex feedback loops and Pulse Width Modulation (PWM), leads to a delayed dynamic response. Additionally, tuning PI or PR parameters is time-consuming, making the controller more intricate. Furthermore, the inherent uncertainties in renewable energy sources lead to fluctuations in the DC-bus voltage in the case of a microgrid, thereby further deteriorating the power quality on the AC side. Consequently, conventional cascaded PI or PR controllers may not effectively address these issues. Moreover, in LCL filter-based two-level inverters with PWM regulators, the stability is significantly influenced by the time delay caused by the modulation process [11]. As a result, implementing compensators and complicated tuning techniques for PI controllers becomes imperative, thereby augmenting the intricacy of the solution [12].

To overcome the traditional controller problems mentioned above, the Model Predictive Control strategy (MPC) has emerged as one of the promising controller solutions due to its fast dynamic response, ease of implementation, and ability to control several parameters for different variables through a single cost function. In addition, MPC is characterized by possibly including constraints in the cost function [13]. Despite that, the conventional MPC suffers from inherent limitations, such as computational complexity, variable switching frequency, average steady-state error, and optimum weighting factor selection [13].

Finite Control Set Model Predictive Control (FCS-MPC) is a type of MPC strategy classified as a direct MPC that controls the converter switches directly. The most significant advantages of this strategy are its fast transient response and its suitability for direct control systems such as (direct torque control) DTC and (direct power control) DPC. However, FCS-MPC is plagued by two significant limitations: the variable switching frequency and computational complexity [14], [15]. Given that the optimization variable in FCS-MPC is represented as an integer, the formulated optimization problem can be classified as a mixed integer program. Consequently, the computational complexity of this problem grows exponentially with the number of candidate solutions. Furthermore, it can become computationally intractable because the FCS-MPC optimization function must be solved in real time, typically within a few tens of microseconds [15].

Several strategies have been developed to reduce the FCS-MPC average computational burden. One of those strategies is proposed in [16] and [17] with one-step prediction horizons (Np=1). In [18], the evaluation of candidate inverter voltage vectors within two consecutive sampling periods is proposed. This approach effectively reduces the computational cost associated with sequential optimization steps. Nevertheless, when higher-order output filters like LCL filters are incorporated, such strategies will fail to track the sinusoidal references, and thus distortions will increase [19].

A comprehensive analysis was conducted in [20] to evaluate the performance of the FCS-MPC algorithm in a grid-connected inverter incorporated with an LCL filter for various state feedback controls and concluded that the prediction horizon longer than 6 with the grid-side current as a control-feedback is the practical solution to overcome the third-order dynamics of the LCL filter. Nevertheless, as mentioned earlier, increasing the prediction horizon length led to an exponential increase in the required calculations.

Multi-objective FCS-MPC strategies have already been proposed in the literature; in such strategies, two or more state variables are controlled using a single cost function. The FCS-MPC algorithm for a grid-connected inverter with LCL filter proposed in [21] considers the capacitor voltage, grid current, and inverter current as state feedback control variables. Furthermore, [19] proposed a different approach, recommending tracking the capacitor voltage reference and its first derivative as control variables feedback for the cost function. However, the presence of weighting factors is the main drawback of this approach, as the values of these factors decisively affect the controller's performance; unfortunately, there is no specific strategy or clear methodology to determine the optimal values of these factors, which makes the controller tuning process a complex and time-consuming task [14]. Therefore, some works in the literature have developed advanced strategies based on artificial intelligence, neural networks, or fuzzy logic techniques to tune these factors [22]-[24]. However, such strategies increase the complexity of the predictive controller design.

However, most existing FCS-MPC schemes for LCL-filtered grid-connected inverters still face a trade-off between computational efficiency and control accuracy. Conventional FCS-MPC with long prediction horizons and multi-objective weighting improves current quality for third-order LCL dynamics, but at the cost of high per-cycle computation and difficult tuning. This paper presents an FCS-MPC strategy that bridges the gap by reducing the prediction horizon from ($N_p = 6$) to ($N_p = 3$), while eliminating weighting factors. By tracking the LCL filter capacitor voltage instead of grid-side current, the proposed method decouples the control loop from the grid's delayed dynamics, enabling shorter horizons without compromising performance. This reduction significantly lowers the number of candidate solutions evaluated per control cycle, making real-time implementation feasible on low-cost embedded platforms. The approach retains the benefits of conventional FCS-MPC, such as fast transient response, while simplifying tuning and enhancing

robustness against grid disturbances. The key contributions of the proposed controller are listed below:

- The proposed method reduced the prediction horizon from Np=6 to Np=3 compared to conventional methods.
- The proposed method implements FCS-MPC using a single-objective cost function without weighting factors, thereby reducing design complexity and eliminating time-consuming tuning.
- The controller effectively eliminates grid current distortion caused by the amplification of high-frequency switching harmonics, which typically arises when tracking the converter-side current.
- It extracts the positive sequence of the PCC voltage and utilizes it exclusively, ensuring sinusoidal current injection even under unbalanced grid voltage conditions.
- The proposed method is validated through real-time embedded implementation using the NI sbRIO GPIC (Single-Board RIO Grid Processor-in-the-Loop Controller) Evaluation Kit.

The remainder of this paper is organized as follows: Section II presents the system description and modeling. Section III provides a brief review of conventional FCS-MPC strategies for GCIs and discusses their associated challenges. In Section IV, the proposed FCS-MPC strategy is introduced in detail. Section V presents both simulation and experimental results that validate the effectiveness, dynamic performance, and robustness of the proposed controller under various operating conditions. Finally, Section VI concludes the paper.

2. System Overview

Fig.1 illustrates the schematic diagram of a two-level three-phase voltage source inverter connected to a grid through an LCL filter. Using Kirchhoff's voltage law (KVL) at the inverter output, the dynamic model of the system is obtained as the following equations:

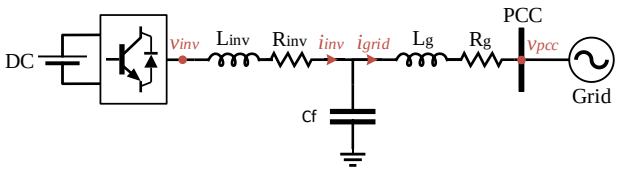

Fig. 1. Single line diagram of the grid-connected inverter with an LCL filter.

$$\frac{di_{inv}}{dt} = \frac{1}{L_{inv}}\left(v_{inv}(t) - i_{inv}(t)R_{inv} - v_c(t)\right) \quad (1)$$

$$\frac{di_{grid}}{dt} = \frac{1}{L_g}\left(v_c(t) - i_{grid}(t)R_g - v_{pcc}(t)\right) \quad (2)$$

$$\frac{dV_c}{dt} = \frac{i_{inv} - i_{grid}}{C_f} \quad (3)$$

Where i_{inv}, and i_{grid} are the inductor currents of the inverter side and the grid side filter, respectively, V_{inv} is the output voltage of the inverter, V_{PCC} is the voltage at PCC, V_c is the filter capacitor voltage, L_{inv} and L_g are the inverter side and the grid side of the LCL output filter, respectively, C_f is the filter capacitor and R_{inv} and R_g are the parasitic resistances of the inductors. This model can be described in a simple State-Space Model form as follows:

$$\dot{x} = Ax + Bu \quad (4)$$

$$x = \begin{bmatrix} i_{inv} \\ i_{grid} \\ v_c \end{bmatrix},\ u = \begin{bmatrix} v_{imv} \\ v_{pcc} \end{bmatrix} \quad (5)$$

$$A = \begin{bmatrix} -\frac{R_{inv}}{L_{inv}} & 0 & -\frac{1}{L_{inv}} \\ 0 & -\frac{R_{grid}}{L_g} & \frac{1}{L_g} \\ \frac{1}{C_f} & -\frac{1}{C_f} & 0 \end{bmatrix} \quad (6)$$

$$B = \begin{bmatrix} \frac{1}{L_{inv}} & 0 \\ 0 & -\frac{1}{L_g} \\ 0 & 0 \end{bmatrix} \quad (7)$$

The discrete-time model of the system described in Eq. (4) can be obtained for the sampling time using the Euler forward method:

$$\begin{bmatrix} i_{inv}(k+1) \\ i_{grid}(k+1) \\ v_c(k+1) \end{bmatrix} \approx A_d \begin{bmatrix} i_{inv}(k) \\ i_{grid}(k) \\ v_c(k) \end{bmatrix} + B_d \begin{bmatrix} v_{imv}(k) \\ v_{pcc}(k) \end{bmatrix} \quad (8)$$

$$A_d = \begin{bmatrix} 1 - \frac{T_s R_{inv}}{L_{inv}} & 0 & -\frac{T_s}{L_{inv}} \\ 0 & 1 - \frac{T_s R_g}{L_g} & \frac{T_s}{L_g} \\ \frac{1}{C_f} & -\frac{1}{C_f} & 0 \end{bmatrix} \quad (9)$$

$$B_d = \begin{bmatrix} \frac{1}{L_{inv}} & 0 \\ 0 & -\frac{1}{L_g} \\ 0 & 0 \end{bmatrix} \quad (10)$$

To ensure sampling-frequency adequacy during the discretization. The system is discretized with forward Euler at the sampling time (T_s) equal to the control/switching period. The T_s should be selected for ($f_s = 1/T_s \geq \kappa f_{\text{res}}$). With:

$$(\kappa \geq 20) \text{ and } f_{\text{res}} = \frac{1}{2\pi}\sqrt{\frac{L_1+L_2}{L_1 L_2 C}}, \text{ and ensure } (f_s \gg f_{\text{grid}}).$$

Hence ($\omega_{\text{res}} T_s \ll 1$), making the Euler local error $\mathcal{O}((\omega T_s)^2)$ negligible for our prediction horizon. The one-sample implementation delay is handled by applying the computed switching state in the next interval.

Moreover, the point of common coupling (PCC) voltage, denoted as v_{pcc}, at the time step (k+n) can be expressed as:

$$\tilde{v}_{pcc}(k+n) = v_{pcc}(k)e^{jn\omega T_s} \quad (11)$$

Here, ω represents the grid angular frequency, while the term ωT_s captures the phase shift of the PCC voltage over a single sampling interval T_s. When the sampling interval is sufficiently small, the PCC voltage can be assumed to remain approximately constant within that interval. Thus,

$$\tilde{v}_{pcc}(k+1) \approx v_{pcc}(k) \quad (12)$$

The relationship between the inverter output voltage v_{inv} and the DC-link voltage V_{dc} is determined by the switching states S of the individual inverter legs. In the $\alpha\beta$ reference frame, this relationship can be described by:

$$v_{inv} = \frac{2}{3} V_{dc}(S_a + aS_b + a^2 S_c) \quad (13)$$

Where, $S_a, S_b, S_c \in \{0,1\}$ are the switching states for the inverter legs (phase A, B, and C, respectively), and a is the complex operator $a = e^{j2\pi/3}$, which represents a 120° phase shift.

3. Conventional FCS-MPC

Finite Control Set Model Predictive Control (FCS-MPC) algorithms directly determine the converter switching signals by formulating the control objectives and system constraints into a cost function. This cost function quantifies the deviation between the desired reference values and the predicted behavior of the system. At each sampling instant, the cost function is evaluated for all feasible switching states of the converter, and the state that minimizes the cost is selected and applied.

For grid-connected inverters (GCIs) employing an LCL output filter, three primary approaches have been reported in the literature for designing the FCS-MPC cost function [20].

The first approach uses the converter-side current as feedback to track the reference current. This method is relatively straightforward and avoids the need for extended prediction horizons (typically $N_p \leq 2$). Moreover, the dynamic nature of the converter-side current can be effectively handled by appropriately designing the LCL filter parameters. However, this method may result in distortion of the grid-side current due to the amplification of high-frequency switching harmonics, which are pronounced near the resonant frequency of the LCL filter. Such distortions may lead to violations of grid code requirements. The associated cost function is given by:

$$g = \left(i_{inv}^{p} - i_{inv}^{*}\right)^2 + g_{lim} \quad (14)$$

Where i_{inv}^{p} and i_{inv}^{*} denote the predicted and reference converter-side currents, respectively, and g_{lim} the constraint penalty term, a function designed to enforce system limits (e.g., capacitor voltage limits, switching frequency reduction, …)

The second approach involves using the grid-side current i_{grid} as feedback. This method simplifies the control of power flow at the PCC by eliminating the need for explicit reactive power compensation. The associated cost function is also simpler:

$$g = \left(i_{grid}^{p} - i_{grid}^{*}\right)^2 + g_{lim} \quad (15)$$

Where i_{grid}^{p} and i_{grid}^{*} denote the predicted and reference grid-side currents, respectively. However, due to the third-order dynamics introduced by the LCL filter, the impact of switching actions on i_{grid} is delayed by at least three sampling intervals (i.e., noticeable at $k+3$). While the filter effectively attenuates high-frequency switching harmonics, this also reduces the responsiveness of the system to switching inputs. As a result, longer prediction horizons are required to maintain performance, leading to a significantly increased computational load.

To address the limitations associated with converter-side current distortion and the computational burden of long horizons, multi-objective FCS-MPC strategies have been proposed. These strategies incorporate multiple feedback variables, either the filter voltage combined with the converter-side current or the filter voltage combined with the grid-side current. The corresponding cost functions are formulated as:

$$g = \lambda_i\left(i_{inv}^{p} - i_{inv}^{*}\right)^2 + \lambda_v\left(v_c^{p} - v_c^{*}\right)^2 + g_{lim} \quad (16)$$

$$g = \lambda_i\left(i_{grid}^{p} - i_{grid}^{*}\right)^2 + \lambda_v\left(v_c^{p} - v_c^{*}\right)^2 + g_{lim} \quad (17)$$

Where, λ_i and λ_v are the weighting factors for the current and capacitor voltage tracking terms, respectively.

While these formulations can improve performance by balancing multiple objectives, they introduce increased complexity in controller design, particularly in the tuning of weighting factors. Moreover, the interplay between different control variables may result in unpredictable performance under varying operating conditions.

All FCS-MPC implementations are subject to time delays introduced by the computational process, which depend on the capabilities of the digital processor used. In modern systems, this delay typically remains below 50 microseconds [25], significantly shorter than that of pulse-width modulation (PWM) based controllers, which can be around 600 microseconds [26]. Nonetheless, to maintain optimal control performance, this delay must be compensated. A practical and effective compensation method is to apply the optimal switching state calculated at the current step in the next time interval [27]. As a result, even in systems where a prediction horizon of $N_p = 1$ would theoretically suffice, extending the horizon to $N_p = 2$ becomes necessary to account for processing delays.

4. Proposed Controller

This study proposes an FCS-MPC strategy that leverages the filter voltage (v_c) for direct tracking of its reference (v_c^*). The approach utilizes a single-objective cost function, thereby eliminating the need for tracking either the converter-side or grid-side current.

As discussed earlier, the switching actions applied to the converter do not produce an immediate effect on the filter voltage. Instead, their influence becomes evident after $N_p = 2$ two discrete time steps. As a result, a minimum prediction horizon of $N_p = 2$ is required to observe any impact of the control input on v_c. Similarly, the control signal applied at $k+1$ influences the filter voltage at $k+3$, effectively requiring a prediction horizon of $N_p = 3$.

To ensure accurate tracking of the reference voltage, it is therefore necessary to predict the values of $v_c(k+2)$ and $v_c(k+3)$. To reduce computational complexity, this paper derives explicit expressions for $v_c(k+2)$ and $v_c(k+3)$ as

direct functions of system variables measured at time step k. This approach eliminates the need for step-by-step recursive calculations from $k+1$through to $k+3$. Utilizing the system dynamics defined in Eqs. (8) – (10), these relationships are analytically derived and presented as follows:

$$v_c(k+2) = \alpha_1 v_{cf}(k) + \alpha_2 i_{inv}(k) + \alpha_3 i_{grid}(k) + \alpha_4 v_{inv}(k) + \alpha_5 v_{PCC}(k) \quad (18)$$

$$v_c(k+3) = \gamma_1 v_{cf}(k) + \gamma_2 i_{inv}(k) + \gamma_3 i_{grid}(k) + \gamma_4 v_{inv}(k) + \gamma_5 v_{inv}(k+1) + \gamma_6 v_{PCC}(k) \quad (19)$$

Where:

$$\alpha_1 = 1 - \frac{T_s^2}{C_f}\left(\frac{1}{L_{inv}} + \frac{1}{L_g}\right), \quad \alpha_2 = \frac{T_s}{C_f}\left(2 - \frac{T_s R_{inv}}{L_{inv}}\right)$$

$$\alpha_3 = -\frac{T_s}{C_f}\left(2 - \frac{T_s R_g}{L_g}\right), \quad \alpha_4 = \frac{T_s^2}{C_f L_{inv}}, \quad \alpha_5 = \frac{T_s^2}{C_f L_g}$$

$$\gamma_1 = 1 - \frac{T_s^2}{C_f}\left(\frac{3}{L_{inv}} + \frac{3}{L_g}\right) + \frac{T_s^3 R_{inv}}{C_f L_{inv}^2} + \frac{T_s^3 R_g}{C_f L_g^2}$$

$$\gamma_2 = \frac{T_s}{C_f}\left(3 - \frac{3T_s R_{inv}}{L_{inv}} + \frac{T_s^2 R_{inv}^2}{L_{inv}^2}\right) - \frac{T_s^3}{C_f L_{inv} L_g}$$

$$\gamma_4 = \frac{T_s^2}{C_f L_{inv}}\left(2 - \frac{T_s R_{inv}}{L_{inv}}\right), \quad \gamma_5 = \frac{T_s^2}{C_f L_{inv}}$$

$$\gamma_6 = -\frac{T_s^2}{C_f L_g}\left(3 - \frac{T_s R_g}{L_g}\right)$$

4.1 Reference Calculation

The primary objective of the proposed grid-following converter control system is to enable decoupled regulation of active and reactive power injected into the grid, thereby allowing operation at a controlled power factor. The relationship between active/reactive power and the point of common coupling (PCC) voltage in the $\alpha\beta$ frame is given by [28]:

$$\begin{bmatrix} P \\ Q \end{bmatrix} = \frac{3}{2}\begin{bmatrix} V_{pcc_\alpha} & V_{pcc_\beta} \\ V_{pcc_\beta} & -V_{pcc_\alpha} \end{bmatrix}\begin{bmatrix} I_{grid_\alpha} \\ I_{grid_\beta} \end{bmatrix} \quad (20)$$

Where V_{pcc_α}, V_{pcc_β} are the $\alpha\beta$ components of the PCC voltage, and I_{grid_α}, I_{grid_β} are the $\alpha\beta$ components of the grid-side current.

Accordingly, the grid-side current components in the $\alpha\beta$ frame can be derived from the desired active P and reactive power Q as:

$$i_{grid_\alpha} = \frac{2P \times v_{pcc_\alpha}}{3\left(v_{pcc_\alpha}^2 + v_{pcc_\beta}^2\right)} + \frac{2Q \times v_{pcc_\beta}}{3\left(v_{pcc_\alpha}^2 + v_{pcc_\beta}^2\right)} \quad (21)$$

$$i_{grid_\beta} = \frac{2P \times v_{pcc_\beta}}{3\left(v_{pcc_\alpha}^2 + v_{pcc_\beta}^2\right)} - \frac{2Q \times v_{pcc_\alpha}}{3\left(v_{pcc_\alpha}^2 + v_{pcc_\beta}^2\right)} \quad (22)$$

These expressions are used to determine the current references required to inject the desired power into the grid. To ensure sinusoidal current injection, only the positive sequence of the PCC voltage is utilized in the computation. Hence, the current references at time step k are given by:

$$i^*_{grid_\alpha}(k) = K_p(k) \times v^+_{pcc_\alpha}(k) + K_q(k) \times v^+_{pcc_\beta}(k) \quad (23)$$

$$i^*_{grid_\beta}(k) = K_p(k) \times v^+_{pcc_\beta}(k) - K_q(k) \times v^+_{pcc_\alpha}(k) \quad (24)$$

Where $v^+_{pcc_\alpha}$, $v^+_{pcc_\beta}$ are the $\alpha\beta$ components of the PCC voltage positive sequence, and K_p, K_q are given as:

$$K_p = \frac{2P^*}{3(V_m^+)^2}, \quad K_q = \frac{2Q^*}{3(V_m^+)^2} \quad (25)$$

And V_m^+ is the positive sequence amplitude of the PCC voltage. Using Eqs. (8) – (10), the grid-side current at time step $k+4$ is predicted as:

$$i_{grid}(k+4) = \frac{T_s}{L_g}\left(V_c(k+3) - R_g i_{grid}(k+3) - v_{pcc}(k+3)\right) + i_{grid}(k+3) \quad (26)$$

Accordingly, the reference filter voltage at $k+3$, required to achieve the desired current injection, is given by:

$$v_c^*(k+3) = \frac{L_g}{T_s}\left(i^*_{grid}(k+4) - i_{grid}(k+3)\right) + R_g i_{grid}(k+3) + v_{pcc}(k+3) \quad (27)$$

4.2 Cost Function Formulation

The proposed FCS-MPC approach employs a single objective cost function focused on minimizing the error between predicted and reference filter voltages. The cost function is defined as:

$$g = \left(v^*_{c_\alpha}(k+3) - v_{c_\alpha}(k+3)\right)^2 + \left(v^*_{c_\beta}(k+3) - v_{c_\beta}(k+3)\right)^2 + g_{i_{lim}} \quad (28)$$

Here, $g_{i_{lim}}$ is a penalty term that discourages excessive voltage magnitudes:

$$g_{i_{lim}} = \begin{cases} \|v_c(k+3)\|; & if \quad \|v_c(k+3)\| \geq V_{max} \\ 0 & otherwise \end{cases} \quad (29)$$

This formulation ensures that under normal conditions, the cost function remains purely focused on voltage tracking, while under constraint violations, it shifts priority to voltage regulation.

4.3 Positive Sequence Extraction

As previously mentioned, the proposed control strategy focuses solely on tracking the positive sequence component of the PCC voltage. This approach ensures sinusoidal current injection into the grid in scenarios of voltage sag or unbalanced grid voltage. The proposed method extracts the positive-sequence component of the PCC voltage using a

discrete-time quadrature signal generator (QSG) and sequence decoupling in the stationary $\alpha\beta$-frame. A harmonic oscillator model generates orthogonal signals $v_{\alpha\beta}^{q}$ from $v_{\alpha\beta}$, governed by:

$$\frac{dv_{\alpha\beta}^{q}}{dt} = -\omega_0 v_{\alpha\beta}, \quad \frac{dv_{\alpha\beta}}{dt} = \omega_0 v_{\alpha\beta}^{q} \tag{30}$$

Discretizing using the Euler-forward method with sampling time T_s:

$$v_{\alpha\beta}(k+1) \approx \omega_0 T_s v_{\alpha\beta}^{q}(k) + v_{\alpha\beta}(k) \tag{31}$$

$$v_{\alpha\beta}^{q}(k+1) \approx -\omega_0 T_s v_{\alpha\beta}(k) + v_{\alpha\beta}^{q}(k) \tag{32}$$

Solving recursively, the quadrature component at step k is:

$$v_{\alpha\beta}^{q}(k) \approx \frac{v_{\alpha\beta}(k) - (\varphi_0^2 T_s^2 + 1) v_{\alpha\beta}(k-1)}{\omega_0 T_s} \tag{33}$$

As evident from Eq. (33), the quadrature voltage component can be readily obtained using only the current and past voltage values. Fortunately, the proposed control strategy inherently provides these values, enabling the extraction of the positive voltage sequence in the frame, as shown below:

$$v_{\alpha}^{+}(k) = \frac{1}{2} v_{\alpha} + \frac{v_{\beta}(k) - (\omega_0^2 T_s^2 + 1) v_{\beta}(k-1)}{2\omega_0 T_s} \tag{34}$$

$$v_{\beta}^{+}(k) = \frac{1}{2} v_{\beta} - \frac{v_{\alpha}(k) - (\omega_0^2 T_s^2 + 1) v_{\alpha}(k-1)}{2\omega_0 T_s} \tag{35}$$

These expressions ensure accurate real-time extraction of the voltage positive sequence using only present and past measurements, making them well-suited for implementation in the proposed predictive control framework.

To mitigate harmonics from LCL resonance or grid distortion, a cascaded moving average filter (MAF) is applied to $v_{\alpha\beta}$ before sequence extraction. The MAF with window length $N_{MAF} = f_s/f_o$ (where $f_s = 1/T_s$) attenuates harmonics at integer multiples of f_o:

$$v_{\alpha\beta}^{flit}(k) = \frac{1}{N_{MAF}} \sum_{n=0}^{N_{MAF}-1} v_{\alpha\beta}(k-n) \tag{36}$$

This pre-filtering ensures robustness against 5th, 7th, and higher-order harmonics common in grid voltages.

Fig.2 illustrates the flowchart of the proposed finite control set model predictive control (FCS-MPC) algorithm, detailing the sequence of control operations executed at each sampling instant.

5. Results and Discussions

5.1 Simulation Results

To evaluate the performance of the proposed controller, a simulation of the system was conducted using MATLAB. The proposed controller's performance with three-step prediction horizons (Np=3) compared to a conventional grid-current-feedback-based FCS-MPC with Np=6, which exhibited the most favourable performance among other conventional controllers.

The steady-state performance of both the proposed and conventional controllers was evaluated under constant reference values of active power ($P = 3\,Kw$) and reactive power ($Q = 0\,var$). Fig.3 illustrates the waveforms of the grid-injected current for both controllers. It can be observed that the proposed controller, with a reduced prediction horizon, achieved a sinusoidal injected current with a THD of 1.7%. This value is remarkably close to the 1.6% THD achieved by the conventional controller with an extended prediction horizon.

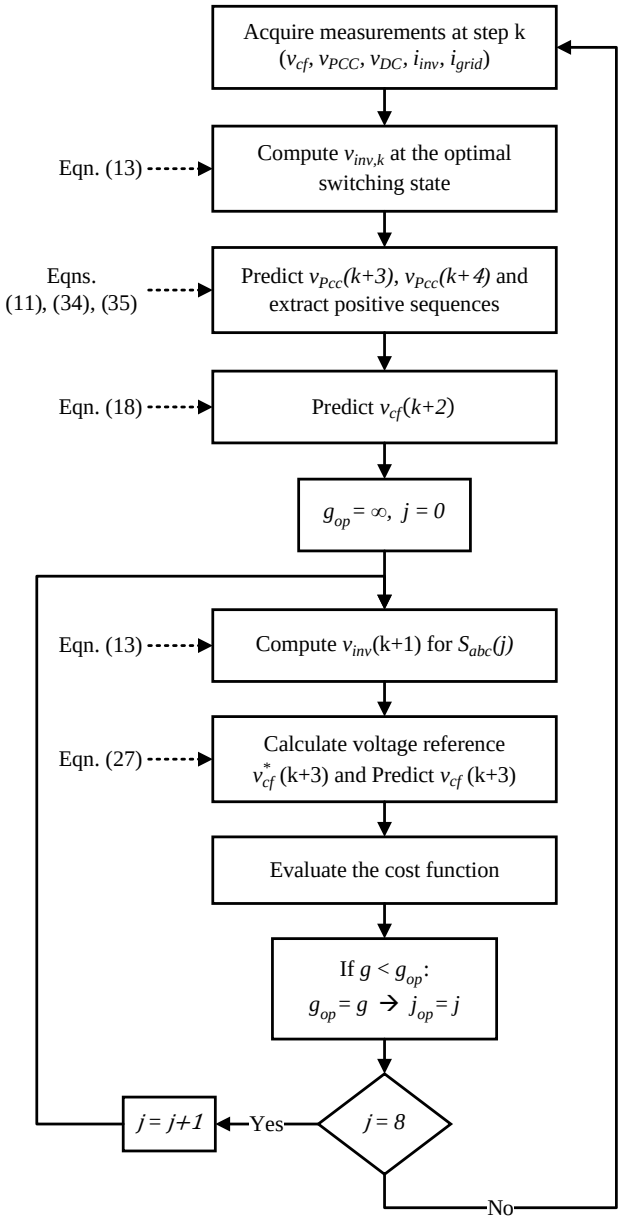

Fig. 2. Flowchart diagram of the proposed control method.

A critical component of testing the robustness of the proposed control system is evaluating its performance under model-plant parameter mismatch, where the parameters used in the predictive model deviate from the actual parameters of the physical system.

LCL filter parameters are the key system parameters that affect the predictive model. To assess the controller robustness under filter parameters mismatch, Simulations were conducted by varying the converter-side inductance, filter capacitance, and grid-side inductance while maintaining the

model parameters themselves. Fig.6 presents the resulting grid-injected current waveforms and their corresponding total harmonic distortion (THD) for the following scenarios: 50% increase and 50% decrease in converter-side inductance, 50% increase and 50% decrease in filter capacitance, and 50% increase and 50% decrease in grid-side inductance. These results illustrate that the system is robust against a wide range of mismatch model parameters.

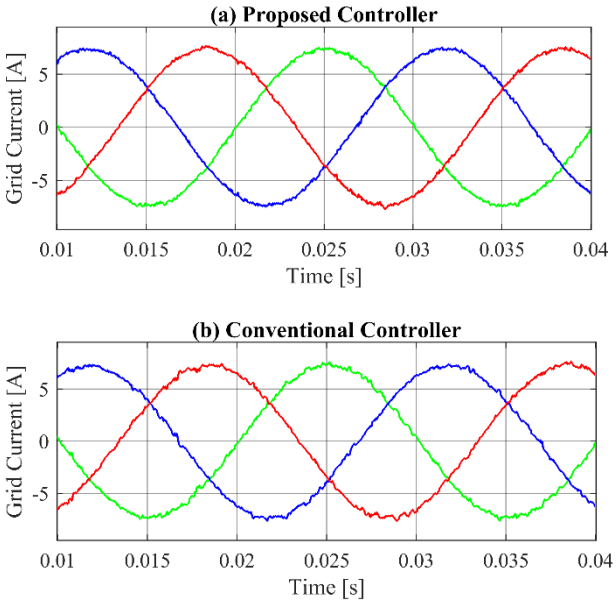

Fig. 3. Steady-state Waveforms of Grid Injected Current Under Stiff Grid Condition: (a) proposed FCS-MPC with Np=3, (b) Conventional grid current feedback-based FCS-MPC with Np=6.

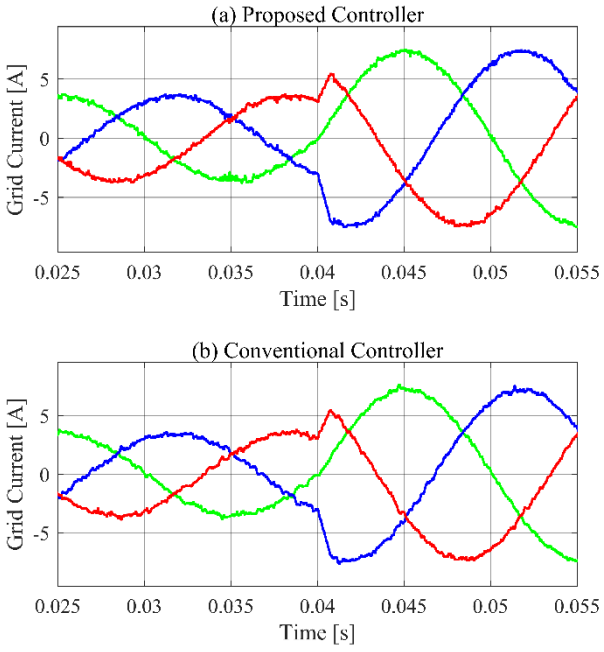

Fig. 4. Transient waveforms of grid injected current for step-up from 1.5 [KW] to 3 [KW] under stiff grid condition: (a) proposed FCS-MPC with Np=3, (b) Conventional grid current feedback-based FCS-MPC with Np=6.

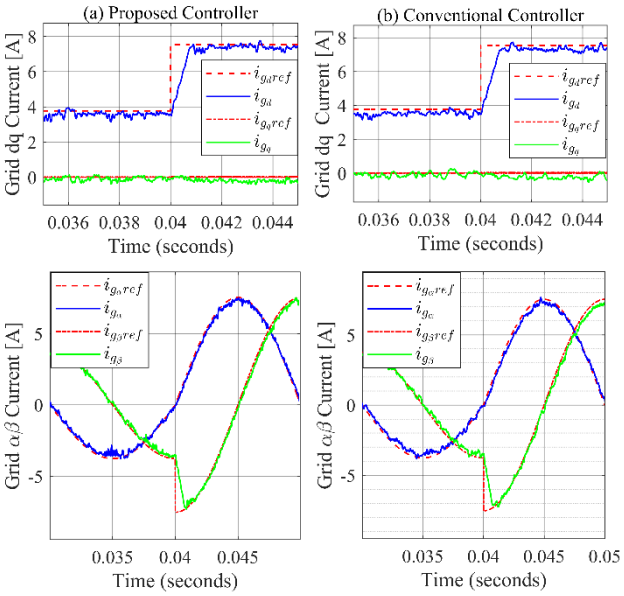

Fig. 5. Transient dq and αβ grid injected current and its references for a step-up from 1.5~kW to 3~kW: (a) Proposed FCS-MPC with N_p=3, (b) Conventional grid current feedback-based FCS-MPC with N_p=6.

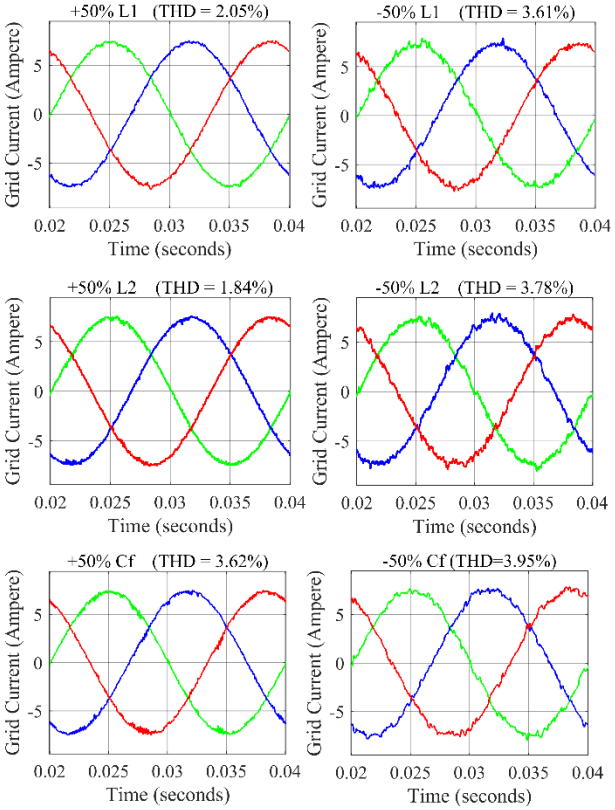

Fig. 6. Grid-injected current waveforms under mismatch parameters.

To further substantiate the robustness of the proposed controller, its performance was evaluated under weak grid conditions, a common scenario characterized by parameter mismatches. In this assessment, the grid inductance was significantly increased from 0.5 mH to 5 mH. Fig.7 presents the waveforms of the PCC voltage, filter voltage, inverter-side current, and grid-injected current. As shown, despite the grid

voltage exhibiting a high harmonic content, with a THD of 6.03%, the proposed controller successfully maintained the injection of a near-sinusoidal current into the grid, achieving a current THD of only 2.01%. This demonstrates the controller's strong resilience to substantial grid impedance variations and weak grid conditions.

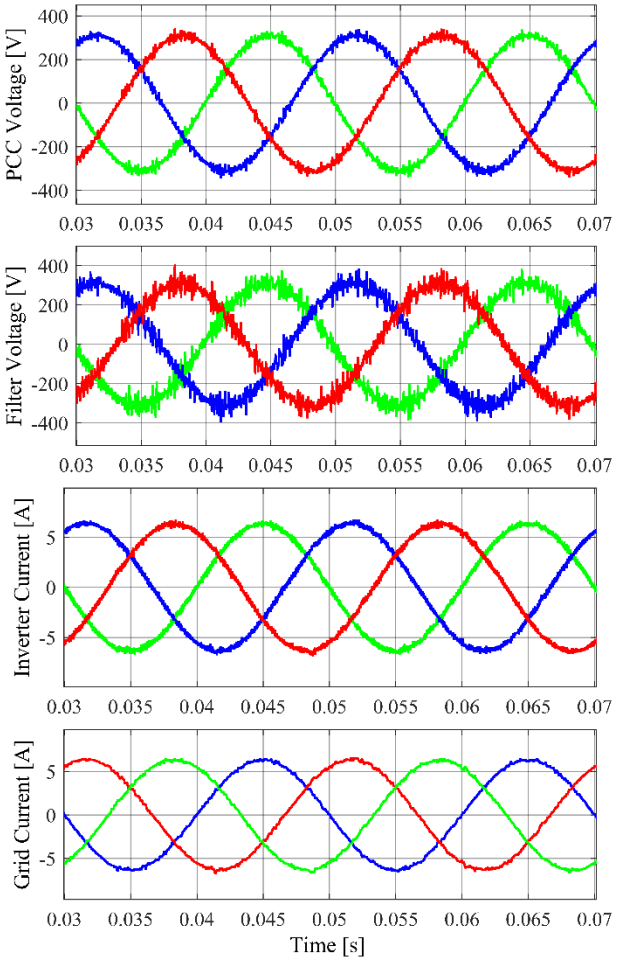

Fig. 7. PCC Voltage, filter voltage, inverter current, and grid-injected current waveforms with grid inductance increased to 5 mH.

To further challenge the system, the grid inductance was increased to $20mH$. In this more severe case, the PCC voltage THD increased to 13.07%, while the grid-injected current THD exhibited only a slight increase to 2.23% as shown in Fig.8, further confirming the effectiveness and robustness of the proposed control strategy under highly adverse grid conditions. Table I summarizes the grid-injected current THD of the proposed FCS-MPC for different operation scenarios.

Table 1. Grid-injected current THD

Op. Scenario	THD_i	Op. Scenario	THD_i
Steady state	1.7%	$+50\%\ L_{grid}$	1.84%
Step change	1.7%	$-50\%\ L_{grid}$	3.78%
$+50\%\ L_{inv}$	2.05%	$+50\%\ C_f$	3.62%
$-50\%\ L_{inv}$	3.61%	$-50\%\ C_f$	3.95%
$Z_g = 5(mH)$	2.01%	$Z_g = 20(mH)$	2.23%

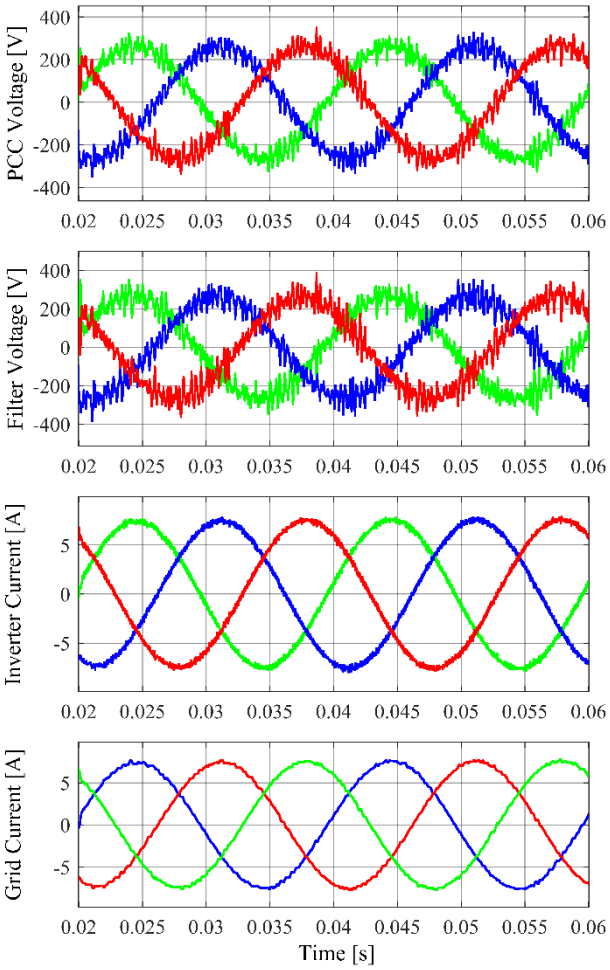

Fig. 8. PCC Voltage, filter voltage, inverter current, and grid-injected current waveforms with grid inductance increased to 20 mH.

As previously described, the proposed controller extracts the reference current based on the positive sequence of the PCC voltage. This design strategy enables the controller to track only the positive sequence component, thereby ensuring that balanced currents are injected into the grid even under unbalanced voltage conditions. To evaluate the controller's performance under such circumstances, simulations were carried out for two test cases.

In the first case, a 30% voltage sag was introduced on phases B and C, occurring between $0.1\ s$ and $0.2s$. Fig.9 illustrates the PCC voltage and the grid-injected current waveforms for this scenario. As shown, the proposed controller successfully maintains the injection of balanced currents into the grid throughout the voltage sag period.

In the second case, the grid voltage was defined with positive and negative sequence components of $(v^+ = 0.5\,pu)$ with a 180-degree phase shift, and $(v^- = 0.3\,pu)$ with a 120-degree phase shift, respectively. This setup emulates a more severe unbalanced voltage sag. The corresponding PCC voltage and grid-injected current waveforms are presented in Fig.10. As observed, the proposed controller effectively maintains balanced current injection into the grid despite the significant voltage imbalance.

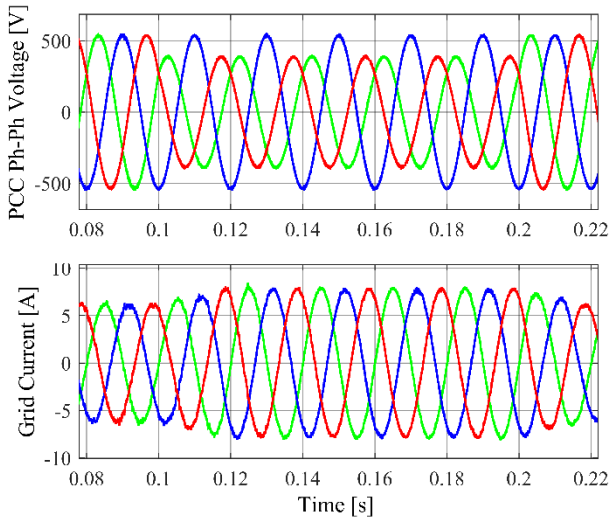

Fig. 9. PCC voltage and grid-injected current waveforms during a 30% voltage sag on phases B and C.

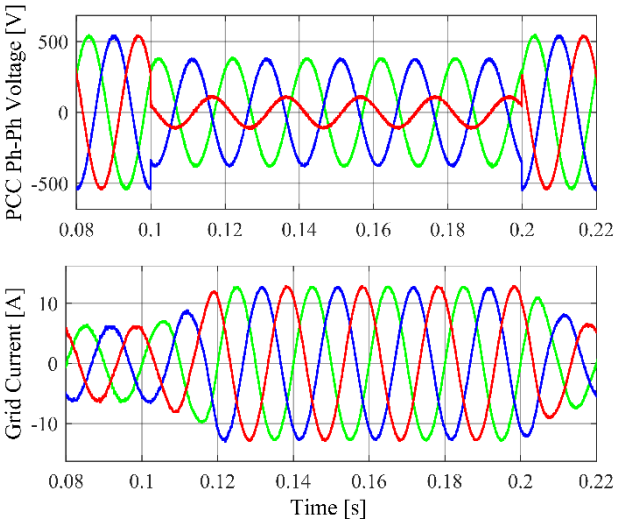

Fig. 10. PCC voltage and grid-injected current waveforms under unbalanced voltage sag with defined positive and negative sequence components.

5.2 Experimental Results

The performance of the proposed controller was experimentally validated using the ECOSENSE Wind Turbine RL Emulator as a real-time embedded system. The experimental setup for this emulator is shown in Fig.11. This system emulates wind turbine behavior by utilizing a DC motor coupled with a permanent magnet synchronous generator (PMSG), along with back-to-back converters and a battery storage system connected through a bidirectional converter to maintain the balance between generation and load. This system utilizes an NI sbRIO GPIC evaluation kit with the sbRIO-9683 RIO Mezzanine Card and the sbRIO-9606 processor and FPGA card as a real-time embedded controller.

The single-line block diagram of the system is presented in Fig.12, and its main parameters are listed in Table II. In this study, a constant wind speed was assumed with constant DC Bus voltage maintained by Turbine-side converter, and the proposed FCS-MPC controller was applied to the grid-side inverter.

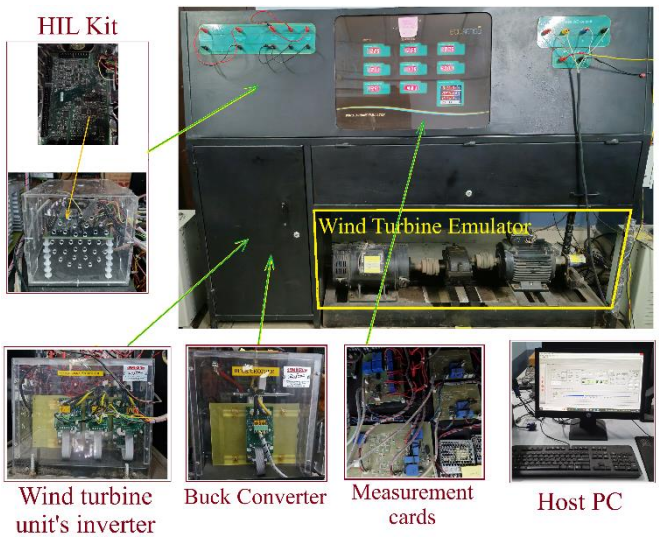

Fig. 11. Experimental setup with some internal parts.

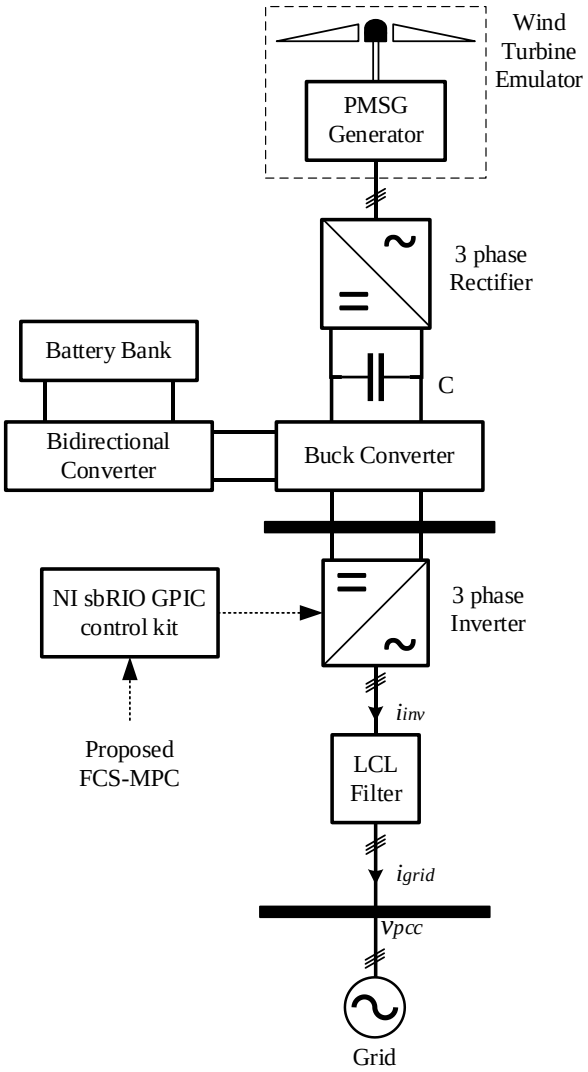

Fig. 12. Block diagram of the experimental setup.

Table 2. Experimental system parameters

Parameter	Value	Description
v_{grid}	380 v	Ph-Ph voltage of the main grid
v_{dc}	500 v	DC bus voltage.
f	50 Hz	Main grid frequency.
T_s	25 μs	Sampling time.
L_{inv}	18 mH	inverter-side inductance of the LCL filter
C_f	25 μF	LCL filter Capacitor
L_g	0.8 mH	Grid-side inductance of the LCL filter

The steady-state performance of the proposed system was experimentally assessed by setting a constant active power reference of 500 [W] while maintaining unity power factor (Q=0 [var]). The corresponding grid-injected current waveforms and instantaneous active power are shown in Fig.13 and Fig.14, respectively. It is evident from the results that the proposed controller, even with a reduced prediction horizon, successfully maintained the desired steady-state behavior and achieved balanced current injection with minimal harmonic distortion. The computational time of the proposed FCS-MPC was measured at 25.3 µs on the 400 MHz sbRIO platform. In stark contrast, the conventional FCS-MPC with Np=6 required 7.8 ms, making it over 300 times slower. This decisive result demonstrates that the proposed method is perfectly suited for real-time implementation on this processor, whereas the conventional approach is computationally prohibitive and would require significantly more powerful hardware.

To further evaluate the dynamic performance of the proposed FCS-MPC controller, the system was subjected to a step change in the active power reference from 500 [W] to 750 [W]. Fig.15 and Fig.16 illustrate the grid-injected current waveforms and the active power response during this transient event. As observed, the controller exhibited excellent reference tracking capability with negligible steady-state error and no observable overshoot, demonstrating its robustness and fast dynamic response under sudden changes in operating conditions.

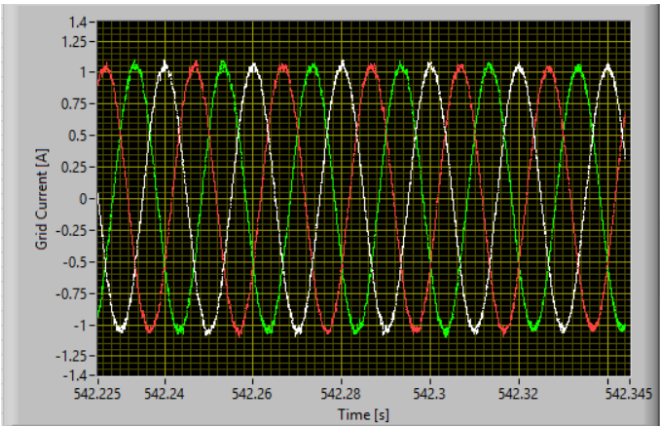

Fig. 13. Experimental result of the grid-injected current in steady state condition.

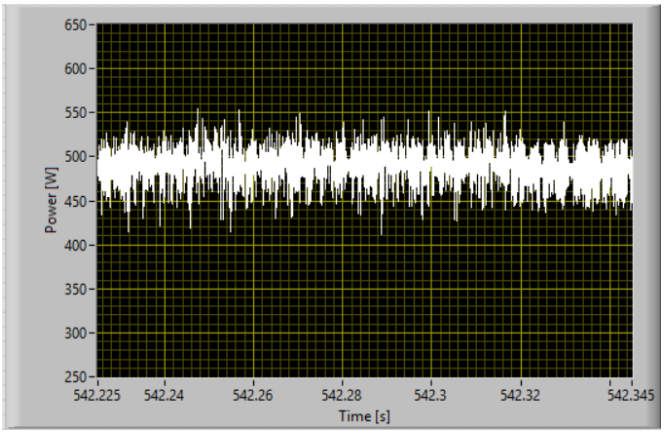

Fig. 14 Experimental result of the active power injected into the grid in steady state condition.

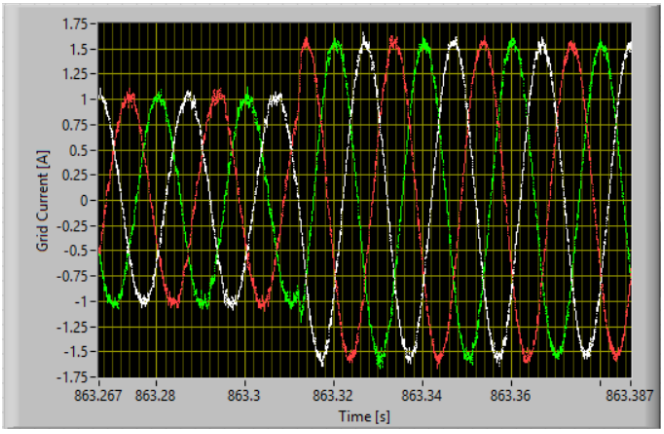

Fig. 15. Experimental result of the grid injected current during step change of the active power reference from 500 to 750 [w]

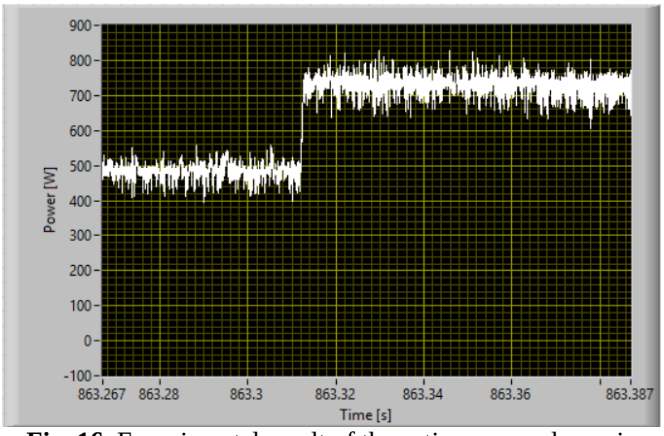

Fig. 16. Experimental result of the active power dynamic response during step change of the active power reference from 500 to 750 [w].

To validate the performance of the proposed FCS-MPC strategy under weak grid conditions, a 5 mH inductance was connected between the grid and the point of common coupling (PCC) to emulate a high grid impedance scenario. The system was operated with an active power reference of 500 [W] while maintaining unity power factor operation, corresponding to a reactive power reference of 0 [VAR]. Fig.17 presents the PCC voltage waveforms under these conditions, where it can be observed that the addition of the inductance introduces

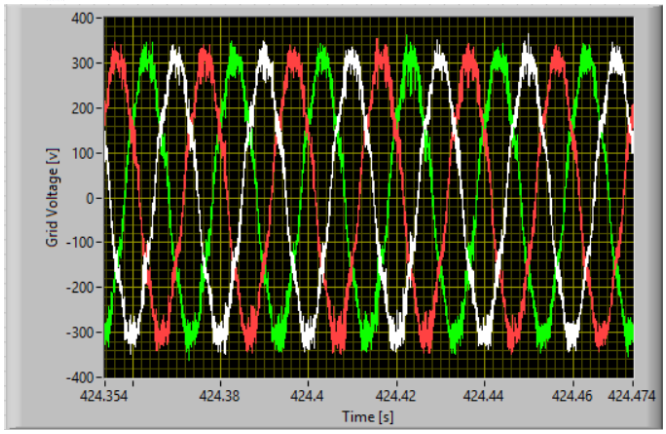

Fig. 17. Experimental result of the PCC voltage under a weak grid condition.

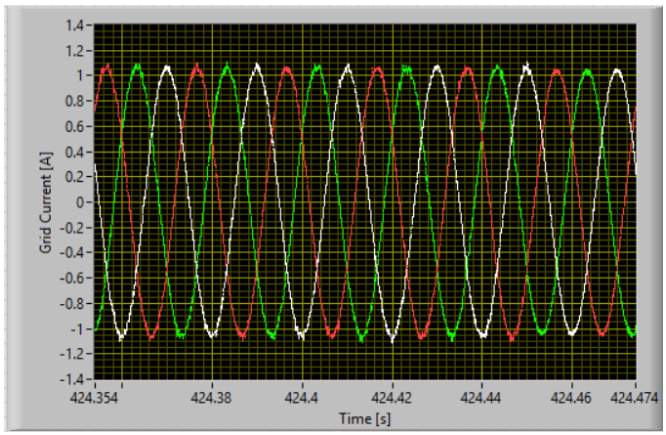

Fig. 18. Experimental result of the grid-injected current under a weak grid condition.

significant distortion into the grid voltage. Despite this adverse condition, the proposed controller effectively maintained stable operation. Fig.18 illustrates the grid-injected current waveforms, demonstrating that the controller successfully regulated the inverter output, preventing the voltage distortion from propagating into the current waveforms. Furthermore, Fig.19 shows the corresponding active power injected into the grid. It is evident that the proposed FCS-MPC controller accurately tracks the active power reference, delivering the commanded power without being affected by the voltage distortion at the PCC. These results confirm the robustness and effectiveness of the proposed control strategy under weak grid conditions.

6. Conclusion

This paper proposed a simple, weighing-factorless finite control set model predictive control (FCS-MPC) strategy for grid-connected microgrids equipped with LCL filters. By tracking the filter capacitor voltage rather than directly controlling the grid-side current, the proposed approach achieved accurate reference tracking with a significantly reduced prediction horizon (Np = 3), thereby addressing the computational complexity issues associated with conventional methods requiring longer horizons and consequently addressed the design complexity by avoiding the weighing factors in the cost function.

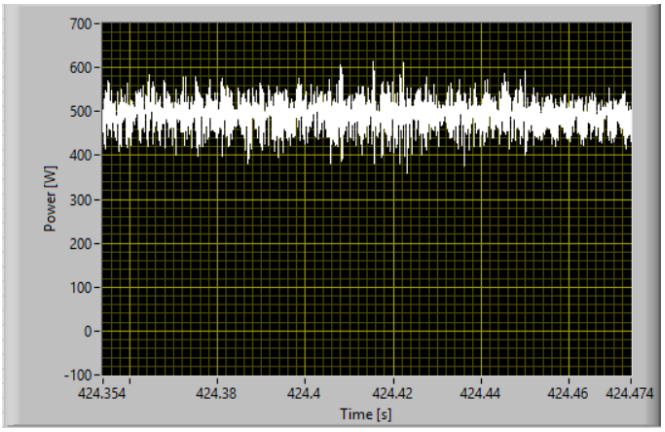

Fig. 19. Experimental result of the instantaneous active power under a weak grid condition.

Both simulation and experimental results validated the effectiveness of the proposed controller under a wide range of operating conditions, including steady-state operation, dynamic power reference changes, parameter mismatches, and weak grid scenarios characterized by high grid impedance and severe voltage distortions.

The performance of the proposed controller is comparable to the conventional method, achieving a grid-current THD of 1.7% in steady-state and 2.23% under a severely weak grid (20 mH grid impedance), while reducing the prediction horizon by 50%. Furthermore, it demonstrated superior steady state and dynamic performance, achieving low injected-current THD, accurate active power tracking, and robust operation without requiring complex weighting factor adjustment. Critically, the experimental implementation confirmed a computational time of just 25.3 µs for the proposed method, over 300 times faster than the 7.8 ms required by the conventional Np=6 approach, making it uniquely suitable for real-time execution on embedded hardware.

Overall, the proposed FCS-MPC strategy offers an efficient and reliable control solution for grid-connected microgrids, ensuring high power quality and reduced computational burden, and showing strong potential for practical deployment in real-world renewable energy integration.

Acknowledgment

The experimental work presented in this paper was supported by the Science and Engineering Research Board (SERB), Government of India, under the Core Research Grant (CRG) project CRG/2018/002041. The support from both institutions is sincerely appreciated.

Author Contributions

A. Tatish was responsible for the conceptualization, data curation, formal analysis, investigation, methodology, validation, writing original draft, review and editing. K. Vaisakh was the project administrator, supervised and guided the overall work. All authors have read and agreed to the published version of the manuscript.

Conflict of Interest

The author(s) declared no potential conflicts of interest with respect to the research, authorship, and/or publication of this article.

References

[1] A. Gulraiz, M. A. Khan, S. Ahmed, and R. Hussain, "Impact of Photovoltaic Ingress on the Performance and Stability of Low Voltage Grid-Connected Microgrids," Results in Engineering, p. 105030, 2025.

[2] M. Ganjian-Aboukheili, M. Shahabi, Q. Shafiee, and J. M. Guerrero, "Linear Quadratic Regulator Based Smooth Transition between Microgrid Operation Modes," IEEE Transactions on Smart Grid, vol. 12, no. 6, pp. 4854–4864, 2021, doi: 10.1109/TSG.2021.3094419.

[3] L. Yang, X. He, P. Zhang, and S. Liu, "Control scheme and performance analysis of dual-frequency single-phase grid-connected inverter interfaced with weak and distorted grids," IEEE Access, vol. 8, pp. 178639–178650, 2020, doi: 10.1109/ACCESS.2020.3022106.

[4] Y. Han, W. Li, H. Lin, and X. Chen, "Modeling and stability analysis of LCL-type grid-connected inverters: A comprehensive overview," IEEE Access, vol. 7, pp. 114975–115001, 2019, doi: 10.1109/ACCESS.2019.2935806.

[5] S. Jahan, S. P. Biswas, S. Haq, M. R. Islam, M. A. P. Mahmud, and A. Z. Kouzani, "An Advanced Control Scheme for Voltage Source Inverter Based Grid-Tied PV Systems," IEEE Transactions on Applied Superconductivity, vol. 31, no. 8, pp. 1–5, 2021, doi: 10.1109/TASC.2021.3094446.

[6] A. Ahmed, S. P. Biswas, M. S. Anower, M. R. Islam, S. Mondal, and S. M. Muyeen, "A Hybrid PWM Technique to Improve the Performance of Voltage Source Inverters," IEEE Access, vol. 11, pp. 4717–4729, 2023, doi: 10.1109/ACCESS.2023.3235791.

[7] S. Kouro, P. Cortés, R. Vargas, U. Ammann, and J. Rodríguez, "Model predictive control - A simple and powerful method to control power converters," IEEE Transactions on Industrial Electronics, vol. 56, no. 6, pp. 1826–1838, 2009, doi: 10.1109/TIE.2008.2008349.

[8] D. M. R. Korada and M. K. Mishra, "Fixed Switching Frequency Model Predictive Current Control for Grid-Connected Inverter With Improved Dynamic and Steady State Performance," IEEE Access, vol. 11, pp. 104094–104105, 2023, doi: 10.1109/ACCESS.2023.3317537.

[9] C. Bao, X. Ruan, X. Wang, W. Li, D. Pan, and K. Weng, "Step-by-step controller design for LCL-Type Grid-Connected inverter with capacitor-current-feedback active-damping," IEEE Transactions on Power Electronics, vol. 29, no. 3, pp. 1239–1253, 2014, doi: 10.1109/TPEL.2013.2262378.

[10] K. H. Ang, G. Chong, and Y. Li, "PID control system analysis, design, and technology," IEEE Transactions on Control Systems Technology, vol. 13, no. 4, pp. 559–576, 2005, doi: 10.1109/TCST.2005.847331.

[11] H. T. Do, X. Zhang, N. V. Nguyen, S. S. Li, and T. T. T. Chu, "Passive-Islanding Detection Method Using the Wavelet Packet Transform in Grid-Connected Photovoltaic Systems," IEEE Transactions on Power Electronics, vol. 31, no. 10, pp. 6955–6967, 2016, doi: 10.1109/TPEL.2015.2506464.

[12] K. T. Tan, P. L. So, Y. C. Chu, and M. Z. Q. Chen, "Coordinated Control and Energy Management of Distributed Generation Inverters in a Microgrid," IEEE Transactions on Power Delivery, vol. 28, no. 2, pp. 704–713, 2013, doi: 10.1109/TPWRD.2013.2242495.

[13] P. Falkowski, A. Sikorski, and M. Malinowski, "Finite control set model predictive control with floating virtual voltage vectors for grid-connected voltage source converter," IEEE Transactions on Power Electronics, vol. 36, no. 10, pp. 11875–11885, 2021, doi: 10.1109/TPEL.2021.3067602.

[14] S. Vazquez, J. Rodriguez, M. Rivera, L. G. Franquelo, and M. Norambuena, "Model Predictive Control for Power Converters and Drives: Advances and Trends," IEEE Transactions on Industrial Electronics, vol. 64, no. 2, pp. 935–947, 2017, doi: 10.1109/TIE.2016.2625238.

[15] P. Karamanakos, M. Nahalparvari, and T. Geyer, "Fixed Switching Frequency Direct Model Predictive Control With Continuous and Discontinuous Modulation for Grid-Tied Converters With LCL Filters," IEEE Transactions on Control Systems Technology, vol. 29, no. 4, pp. 1503–1518, 2020, doi: 10.1109/TCST.2020.3008030.

[16] P. Cortes, G. Ortiz, J. I. Yuz, J. Rodriguez, S. Vazquez, and L. G. Franquelo, "Model predictive control of an inverter with output LC filter for UPS applications," IEEE Transactions on Industrial Electronics, vol. 56, no. 6, pp. 1875–1883, 2009, doi: 10.1109/TIE.2009.2015750.

[17] V. Yaramasu, M. Rivera, M. Narimani, B. Wu, and J. Rodriguez, "Model predictive approach for a simple and effective load voltage control of four-leg inverter with an output LC filter," IEEE Transactions on Industrial Electronics, vol. 61, no. 10, pp. 5259–5270, 2014, doi: 10.1109/TIE.2013.2297291.

[18] P. Cortes, J. Rodriguez, S. Vazquez, and L. G. Franquelo, "Predictive control of a three-phase UPS inverter using two steps prediction horizon," Proceedings of the IEEE International Conference on Industrial Technology, pp. 1283–1288, 2010, doi: 10.1109/ICIT.2010.5472535.

[19] T. Dragicevic, "Model Predictive Control of Power Converters for Robust and Fast Operation of AC Microgrids," IEEE Transactions on Power Electronics, vol. 33, no. 7, pp. 6304–6317, 2018, doi: 10.1109/TPEL.2017.2744986.

[20] N. Panten, N. Hoffmann, and F. W. Fuchs, "Finite Control Set Model Predictive Current Control for Grid-Connected Voltage-Source Converters with LCL Filters: A Study Based on Different State Feedbacks," IEEE Transactions on Power Electronics, vol. 31, no. 7, pp. 5189–5200, 2016, doi: 10.1109/TPEL.2015.2478862.

[21] P. Falkowski and A. Sikorski, "Finite Control Set Model Predictive Control for Grid-Connected AC-DC Converters with LCL Filter," IEEE Transactions on Industrial Electronics, vol. 65, no. 4, pp. 2844–2852, 2018, doi: 10.1109/TIE.2017.2750627.

[22] A. Bakeer and I. S. Mohamed, "An Artificial Neural Network-Based Model Predictive Control for Three-Phase Flying Capacitor Multilevel Inverter," IEEE Access, vol. 10, pp. 70305–70316, 2022, doi: 10.1109/ACCESS.2022.3187996.

[23] M. Babaie, K. Al-Haddad, and L. Franquelo, "Self-Training Intelligent Predictive Control for Power Converters," IEEE Transactions on Power Electronics, vol. 38, no. 1, pp. 12482–12496, 2023, doi: 10.1109/TPEL.2023.3293820.

[24] L. Tang, W. Xu, X. Wang, D. Dong, X. Xiao, and Y. Zhang, "Weighting Factors Optimization of Model Predictive Control Based on Fuzzy Thrust Constraints for Linear Induction Machine," IEEE Transactions on Applied Superconductivity, vol. 31, no. 8, pp. 1–5, 2021, doi: 10.1109/TASC.2021.3103704.

[25] S. Vazquez, J. Rodriguez, M. Rivera, L. G. Franquelo, and M. Norambuena, "Model predictive control: A review of its applications in power electronics," IEEE Industrial Electronics Magazine, vol. 8, no. 1, pp. 16–31, 2014, doi: 10.1109/MIE.2013.2290138.

[26] B. H. Bae and S. K. Sul, "A compensation method for time delay of full-digital synchronous frame current regulator of PWM AC drives," IEEE Transactions on Industry Applications, vol. 39, no. 3, pp. 802–810, 2003, doi: 10.1109/TIA.2003.810660.

[27] P. Cortes, J. Rodriguez, C. Silva, and A. Flores, "Delay compensation in model predictive current control of a three-phase inverter," IEEE Transactions on Industrial Electronics, vol. 59, no. 2, pp. 1323–1325, 2012, doi: 10.1109/TIE.2011.2157284.

[28] E. Pouresmaeil, C. Miguel-Espinar, M. Massot-Campos, D. Montesinos-Miracle, and O. Gomis-Bellmunt, "A control technique for integration of DG units to the electrical networks," IEEE Transactions on Industrial Electronics, vol. 60, no. 7, pp. 2881–2893, 2013, doi: 10.1109/TIE.2012.2209616.